高等学校化学学报
CHEMICAL JOURNAL OF CHINESE UNIVERSITIES
研究论文

# 基于双极聚集诱导延迟荧光材料制备高效稳定厚膜非掺杂有机发光二极管

秦嘉怡[1], 陈紫薇[1], 曾嘉杰[1], 付　燕[1], 唐本忠[2], 赵祖金[1]
(1. 华南理工大学发光材料与器件全国重点实验室, 广东省分子聚集发光重点实验室, 广州 510640;
2. 香港中文大学(深圳)理工学院, 广东省高等学校聚集体科学基础研究卓越中心, 深圳 518172)

**摘要**　厚膜有机发光二极管(OLED)是由一层厚膜同时行使载流子传输与发光功能的器件, 在简化制备工艺和提升工作稳定性方面优势显著. 然而, 要获得高效的非掺杂厚膜OLED器件, 发光材料必须兼具平衡的双极载流子传输特性, 高固态发光效率和高激子利用率, 对发光材料的设计提出了更高的要求. 本研究选取2个代表性的双极聚集诱导延迟荧光(AIDF)材料应用于此类器件的制备. 基于这些材料制备的厚膜器件表现出优异的电致发光性能, 具有启亮电压低(约2.5 V), 外量子效率高(达19.8%), 以及高亮度下效率滚降非常低等优点. 此外, 厚膜器件的工作寿命比薄膜器件提升了2倍以上. 这些厚膜还可以敏化窄光谱多重共振发光材料来制备高效率、高色纯度、结构简化的厚膜超荧光OLED器件. 以上结果表明, 该双极AIDF材料是制备简易厚膜OLED器件的有潜力的候选材料. 本研究为开发高效稳定的OLED器件提供了一个新策略.

**关键词**　聚集诱导延迟荧光; 有机发光二极管; 厚膜非掺器件; 平衡双极载流子传输; 超荧光
**中图分类号**　O632　　**文献标志码**　A　　doi: 10.7503/cjcu20260011

# Efficient and Stable Thick-layer Non-doped Organic Light-emitting Diodes Based on Bipolar Aggregation-induced Delayed Fluorescence Materials

QIN Jiayi[1], CHEN Ziwei[1], ZENG Jiajie[1], FU Yan[1*], TANG Ben Zhong[2], ZHAO Zujin[1*]
(*1. State Key Laboratory of Luminescent Materials and Devices, Guangdong Provincial Key Laboratory of Luminescence from Molecular Aggregates, South China University of Technology, Guangzhou* 510640, *China*;
*2. Guangdong Basic Research Center of Excellence for Aggregate Science, School of Science and Engineering, the Chinese University of Hong Kong, Shenzhen, Shenzhen* 518172, *China*)

**Abstract**　Thick-layer organic light-emitting diodes (OLEDs) comprising a single thick film to simultaneously transport carriers and emit light offer significant advantages in simplifying the fabrication process and enhancing operational stability. However, achieving highly efficient thick-layer non-doped OLEDs requires emitters possessing balanced bipolar carrier transport, strong solid-state emission and high exciton utilization, which impose high requirements on designing luminescent materials. In this work, two representative bipolar aggregation-induced delayed fluorescence (AIDF) emitters are employed to fabricate such thick-layer non-doped devices. Excellent

收稿日期: 2026-01-04. 网络首发日期: 2026-02-22.
联系人简介: 赵祖金, 男, 博士, 教授, 主要从事有机光电功能材料与器件、聚集诱导发光方面的研究. E-mail: mszjzhao@scut.edu.cn
付　燕, 女, 博士, 主要从事有机发光材料的开发和应用方面的研究. E-mail: fyscut@scut.edu.cn
基金项目: 国家自然科学基金(批准号: U23A20594、2375066)、广东省基础与应用基础研究基金项目(批准号: 2023B1515040003)和华南理工大学发光材料与器件全国重点实验室基金(批准号: Skllmd-2024-06)资助.
Supported by the National Natural Science Foundation of China(Nos.U23A20594, 22375066), the Guangdong Basic and Applied Basic Research Foundation, China(No. 2023B1515040003) and the Foundation of State Key Laboratory of Luminescent Materials and Devices, South China University of Technology, China(No.Skllmd-2024-06).

electroluminescence (EL) performances are attained with low turn-on voltages (2.5 V), high external quantum efficiencies (19.8%), and negligible efficiency roll-off at high luminance. Furthermore, the operational lifetime of the thick-layer device increases by more than twofold compared to that of the thin-layer devices. In addition, high-efficiency, high-color-purity simplified thick-layer hyperfluorescence OLEDs are also achieved by using their thick neat films as sensitizers for multi-resonance emitters. These results indicate that the bipolar AIDF emitters are promising candidates for constructing simple thick-layer OLEDs, which provides a feasible strategy for developing highly efficient and stable OLEDs.

**Keywords** Aggregation-induced delayed fluorescence; Organic light-emitting diode(OLED); Thick-layer non-doped OLED; Balanced bipolar charge transport; Hyperfluorescence

## 1 Introduction

Organic light-emitting diodes (OLEDs) have been widely applied in displays, owing to their unique advantages such as high contrast, flexibility, and fast response[1—3]. They also hold promise for solid-state lighting and flexible electronic devices[4—6]. Traditional high-performance OLEDs typically feature a multi-layer configuration to facilitate charge injection, transport and exciton confinement[7,8]. This requires incorporating various functional layers, including hole-transporting layers (HTL), electron-transporting layers (ETL), hole-blocking layers (HBL), and electron-blocking layers (EBL). However, the multiplication of functional layers not only increases the fabrication complexity but also may induce defect states and joule heat at interfaces, thereby degrading the operational stability of OLEDs[9,10]. Encouragingly, the simple thick-layer device featuring eliminated functional layers and thickened emitting layer (EML) has emerged and proven to be a viable strategy for enhancing device stability[11,12].

Tracing the development of thick-layer OLEDs, the first example of thick-layer OLEDs with competitive electroluminescence (EL) performance with traditional multilayer devices was reported by Wang *et al.* in 2012[13]. Subsequently, Blom *et al.* [11] performed a systematic study on thick-layer OLEDs based on emitter CzDBA, confirming that the thick EML can broaden the exciton recombination zone and reduce the exciton concentration, thereby suppressing the bimolecular annihilation of excitons, such as triplet-triplet annihilation (TTA) and triplet-polaron annihilation (TPA). Additionally, the lowered defect density and balanced carrier injection afforded by interface engineering are also conducive to improving the stability of thick-layer OLEDs[14—16]. Given that the thick-layer device requires EML materials to perform light-emitting and charge-transporting functions simultaneously, several studies have also focused on the structural modulation of emitters to improve the EL performance of thick-layer devices[12,17,18]. The core requirements for emitters used in thick-layer devices have been gradually clarified. Firstly, the carrier transport distance increases significantly in thick films, and any inadequacy in charge transport capability or imbalance in electron/hole mobility would lead to increased driving voltage and reduced exciton recombination efficiency[18,19]. Secondly, the aggregation-caused quenching (ACQ) effect that usually occurs at high concentrations or in solid states would cause a substantial reduction in photoluminescence quantum yield ($\Phi_{PL}$)[20—22]. Therefore, novel luminescent materials that simultaneously possess efficient solid emission, balanced bipolar charge transport capability, anti-aggregation quenching property as well as high exciton utilization are the key to afford high-performance thick-layer OLEDs[17].

Recently, aggregation-induced emission (AIE) and aggregation-induced delayed fluorescence (AIDF) emitters have attracted considerable interest because of their excellent solid-emission property and impressive advantages in the fabrication of highly efficient non-doped OLEDs[23—27], which provide a feasible pathway to alleviate the ACQ issue in such thick-layer devices. The purely organic AIDF emitters could harness the

triplet excitons *via* the reverse intersystem crossing (RISC) process, thereby achieving near-unity exciton utilization[28—31]. Small singlet-triplet energy splitting ($\Delta E_{ST}$) would facilitate the RISC process and provide efficient delayed fluorescence[32]. Therefore, the AIDF emitter typically employs a twisted donor-acceptor (D-A) structure, which leads to spatial separation of the highest occupied molecular orbital (HOMO) and the lowest unoccupied molecular orbital (LUMO) to reduce $\Delta E_{ST}$. In 2018, our group integrated the AIDF unit with host materials including 1,4-di(carbazol-9-yl)benzene (DCB), 4,4′-bis(carbazol-9-yl)biphenyl (CBP), 1,3-bis(carbazol-9-yl)benzene (*m*CP) and 3,3′-di(carbazol-9-yl)biphenyl (*m*CBP), and synthesized four molecules, DCB-BP-PXZ, CBP-BP-PXZ, *m*CP-BP-PXZ and *m*CBP-BP-PXZ[33]. The incorporation of host materials mitigates concentration quenching at high voltage and enhances carrier transport, thereby endowing the non-doped OLEDs based on these AIDF emitters with brilliant EL efficiency and negligible efficiency roll-off.

In this work, two AIDF emitters, *m*CP-BP-PXZ and *m*CBP-BP-PXZ, with more balanced carrier mobility relative to DCB-BP-PXZ and CBP-BP-PXZ are selected and applied in simple thick-layer non-doped devices (Fig. 1). Both materials have merits of possessing high $\Phi_{PL}$s, small $\Delta E_{ST}$s and fast RISC processes in neat films. After screening the HBL/EBL materials and modulating the thickness of EML, the thick-layer non-doped OLEDs achieve excellent EL performances with the maximum external quantum efficiencies ($EQE_{max}$) of up to 19.8% and efficiency roll-off of 3.0% at 1000 cd/m$^2$. Furthermore, the resulting broadened recombination zone and reduced exciton density contribute to significantly enhanced operational stability of these thick-layer devices. These results would provide valuable guidance for the development of highly efficient and stable OLEDs.

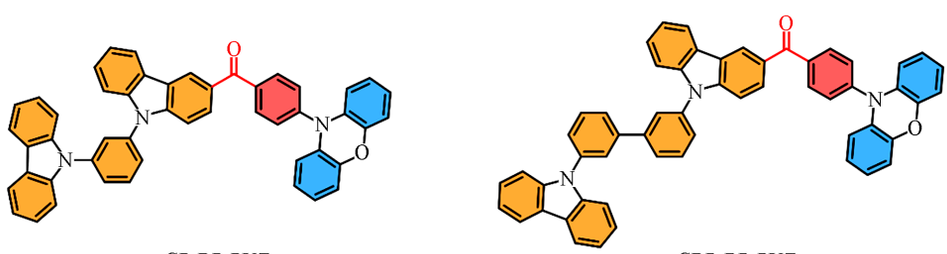


*m*CP-BP-PXZ　　*m*CBP-BP-PXZ

**Fig. 1　Molecular structures of AIDF emitters *m*CP-BP-PXZ and *m*CBP-BP-PXZ**

## 2　Experimental

### 2.1　Synthesis and Characterization

All the chemicals are purchased from commercial sources and used as received without further purification. The synthetic routes of *m*CP-BP-PXZ and *m*CBP-BP-PXZ were performed according to the literature[33]. The final products were subjected to vacuum sublimation to further improve purity before photoluminescence (PL) and EL properties investigations.

### 2.2　Photophysical Measurements

Toluene solutions of *m*CP-BP-PXZ and *m*CBP-BP-PXZ ($10^{-5}$ mol/L) were prepared to explore the absorption and PL characteristics in the solution state. Neat films were deposited on quartz glass substrates by vacuum evaporation to study the solid emission properties. Ultraviolet-visible absorption and photoluminescence spectra were recorded on a UV-2600 ultraviolet-visible spectrophotometer (Shimadzu, Japan) and a Fluoromax-4 fluorescence spectrometer (Horiba, Japan). Absolute PL quantum yields were measured on a Quantaurus-QY measurement integrating sphere (C11347-11, Hamamatsu Photonics) under a nitrogen atmosphere. The transient PL decay curves were recorded using an FLS 1000 photoluminescence spectrometer (Edinburgh, UK) under a nitrogen atmosphere.

### 2.3 OLED Fabrication and Characterization

The glass substrates precoated with a 90 nm layer of indium tin oxide (ITO) with a sheet resistance of 15—20 Ω per square were successively cleaned in an ultrasonic bath of acetone, isopropanol, detergent, and deionized water, respectively, taking 10 min for each step. Then, the substrates were dried in an oven at 70 °C for at least 6 h. Before the fabrication processes, to improve the hole injection ability of ITO, the substrates were treated by $O_2$ plasma for 10 min. The vacuum-deposited OLEDs were fabricated under the pressure of $5\times10^{-4}$ Pa in the OMV-FS380 vacuum deposition system. Deposition rates were controlled by independent quartz crystal oscillators, which were 0.1—0.2 nm/s for organic materials, 0.03 nm/s for $MoO_3$, 0.01 nm/s for LiF, and 0.2 nm/s for Al, respectively. The emission area of the devices was 9 $mm^{-2}$ as shaped by the overlapping area of the anode and cathode. The EL spectra, external quantum efficiencies (EQEs), and luminance-voltage-current density (L-V-J) characteristics of the devices were measured by a PR-670 spectroradiometer equipped with a Keithley 2400 source meter. All the device characterization steps were carried out at room temperature under ambient laboratory conditions without encapsulation except for device lifetime measurement, as soon as the devices were fabricated. In addition, the operational lifetime of OLED devices was measured at a constant direct current at room temperature with an initial luminance of 1000 cd/$m^2$. All devices were immediately encapsulated by UV adhesive LT-U001 using the UV light-exposure system ELC-50 in the nitrogen-filled glove box [$O_2$<1 ppm (parts per million) and $H_2O$<1 ppm (parts per million)] for 3 min.

## 3 Results and Discussions

### 3.1 Photophysical Properties

The photophysical properties of *m*CP-BP-PXZ and *m*CBP-BP-PXZ are studied in dilute toluene solutions ($10^{-5}$ mol/L) and neat films with a thickness of 60 nm (Fig.2). In toluene solutions, the absorption maxima of

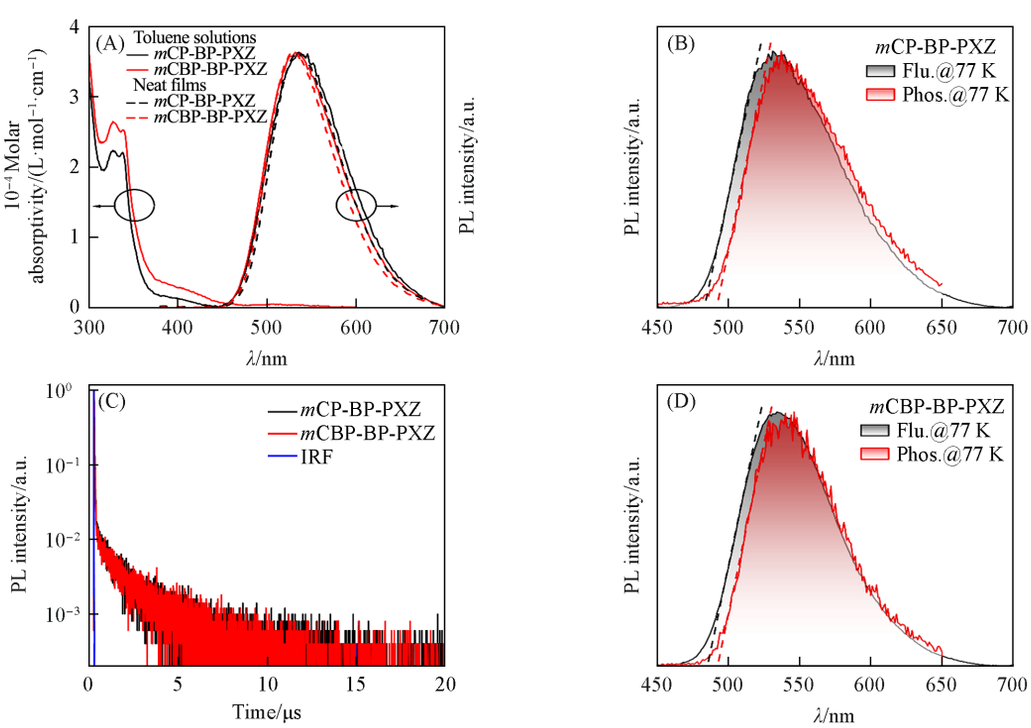


**Fig. 2 Absorption and PL spectra of *m*CP-BP-PXZ and *m*CBP-BP-PXZ in toluene solutions and PL spectra in neat films measured at room temperature(A), fluorescence and phosphorescence spectra of *m*CP-BP-PXZ(B) and *m*CBP-BP-PXZ(D) in neat films measured at 77 K under nitrogen, transient PL decay curves of *m*CP-BP-PXZ and *m*CBP-BP-PXZ in neat films(C) at room temperature**

*m*CP-BP-PXZ and *m*CBP-BP-PXZ are located at around 338 nm, associated with the $\pi$-$\pi^*$ transition, and the broad absorption tail between 375 and 435 nm can be attributed to the intramolecular charge transfer (ICT) transition from the electron-donor phenoxazine (PXZ) to the electron-acceptor carbonyl group. PL spectra in toluene solutions exhibit the PL emission peaks ($\lambda_{PL}$s) at 536 nm for *m*CP-BP-PXZ and 532 nm for *m*CBP-BP-PXZ. In neat films, the $\lambda_{PL}$s of *m*CP-BP-PXZ and *m*CBP-BP-PXZ are similar with those in solutions, which are 535 and 532 nm, respectively. From the onset of the fluorescence and phosphorescent spectra recorded at 77 K, the singlet and triplet energies are obtained to be 2.567 and 2.522 eV for *m*CP-BP-PXZ, and 2.553 and 2.520 eV for *m*CBP-BP-PXZ [Figs. 2(B) and (C)]. Small $\Delta E_{ST}$s of 0.045 eV for *m*CP-BP-PXZ and 0.033 eV for *m*CBP-BP-PXZ are calculated, which can accelerate the RISC process and thus improve the utilization of triplet excitons[34]. The $\Phi_{PL}$s of *m*CP-BP-PXZ and *m*CBP-BP-PXZ are measured to be 82.9% and 97.4% in neat films, respectively. The suppressed concentration quenching can be attributed to their brilliant AIDF properties[33]. The transient PL decay spectra of *m*CP-BP-PXZ and *m*CBP-BP-PXZ are recorded in neat films under nitrogen. As shown in Fig. 2(D), the transient PL decay curves of these emitters exhibit typical double-exponential characteristics with a nanosecond-scale prom pt fluorescence and a microsecond-scale delayed fluorescence. The short lifetime of delayed fluorescence (1.46 and 1.49 μs) affords fast RISC process ($k_{RISC}$) of $1.20\times10^6$ $s^{-1}$ for *m*CP-BP-PXZ and $1.14\times10^6$ $s^{-1}$ for *m*CBP-BP-PXZ (Table 1), endowing triplet excitons with efficient up-conversion[35—37].

**Table 1 Photophysical Data of *m*CP-BP-PXZ and *m*CBP-BP-PXZ**

| Emitter | Toluene Solutions[a] | | Neat films[b] | | | | | | | |
|---|---|---|---|---|---|---|---|---|---|---|
| | $\lambda_{abs}$[c]/nm | $\lambda_{em}$[d]/nm | $\lambda_{em}$[d]/nm | $\Delta E_{ST}$[e]/eV | $\Phi_{PL}$[f](%) | $\tau_{PF}$[g]/ns | $\tau_{DF}$[g]/μs | $R_{DF}$[h](%) | $10^{-7}k_F$[i]/$s^{-1}$ | $10^{-6}k_{RISC}$[j]/$s^{-1}$ |
| *m*CP-BP-PXZ | 338 | 536 | 535 | 0.045 | 82.9 | 22.51 | 1.46 | 43.0 | 2.10 | 1.20 |
| *m*CBP-BP-PXZ | 338 | 532 | 532 | 0.033 | 97.4 | 21.96 | 1.49 | 41.2 | 2.61 | 1.14 |

*a*. Measured in toluene solutions($10^{-5}$ mol/L) at room temperature; *b*. measured in neat films at room temperature; *c*. maximum absorption; *d*. Peak value of PL spectrum; *e*. estimated from the high-energy onsets of fluorescence and phosphorescence spectra at 77 K; *f*. determined in neat films by a calibrated integrating sphere in nitrogen at room temperature; *g*. lifetimes calculated from the prompt component($\tau_{PF}$) and delayed component($\tau_{DF}$) fluorescence decay, respectively; *h*. ratio of delayed component calculated from transient PL decay curves; *i*. fluorescence decay rate calculated from the equations given in the Section 2 of the Supporting Information; *j*. rate constant of RISC calculated from the equations given in the Section 2 of the Supporting Information.

In view of the higher horizontal transition dipole ratio ($\Theta_{//}$), which is conducive to improving the light out-coupling efficiency ($\eta_{out}$)[38—40], the dipole orientation behaviors of *m*CP-BP-PXZ and *m*CBP-BP-PXZ in neat films (50 nm) are evaluated by collecting the *p*-polarized PL signals at different detection angles (0°—90°). The $\Theta_{//}$ values of *m*CP-BP-PXZ and *m*CBP-BP-PXZ are 71.0% and 72.1%, respectively, indicating the enhanced $\eta_{out}$s relative to those of conventional emitters with random dipole orientation ($\Theta_{//}$=66.7%). The improved anisotropy can be attributed to the introduction of *m*CP and *m*CBP groups, which expand the molecular plane and elongate the molecular length, thereby promoting the in-plane alignment of emitters[40,41]. To investigate the influence of EML thickness on $\Theta_{//}$, the neat films with thicknesses of 50, 60, 70 and 80 nm are further prepared. As shown in Fig. S1 (see the Supporting Information of this paper), the $\Theta_{//}$ only deviates slightly across different thicknesses, but the overall variation is limited. Based on $\Theta_{//}$, the reflex index and active layer thickness, the $\eta_{out}$s of thick-layer devices with EML thicknesses ranging from 50 to 80 nm are simulated *via* the Finite Difference Time Domain (FDTD) method (Fig. S2, see the supporting information of this paper). Without considering the recombination profile, both $\eta_{out}$s are dependent on the emissive position and the cavity thickness. With the thickness increasing from 50 to 80 nm, the maximum $\eta_{out}$s are significantly improved from 23.8% to 28.6% for *m*CP-BP-PXZ and 24.2% to 28.5% for *m*CBP-BP-PXZ, demonstrating that the thick-layer structure facilitates constructive interference and enhances $\eta_{out}$.

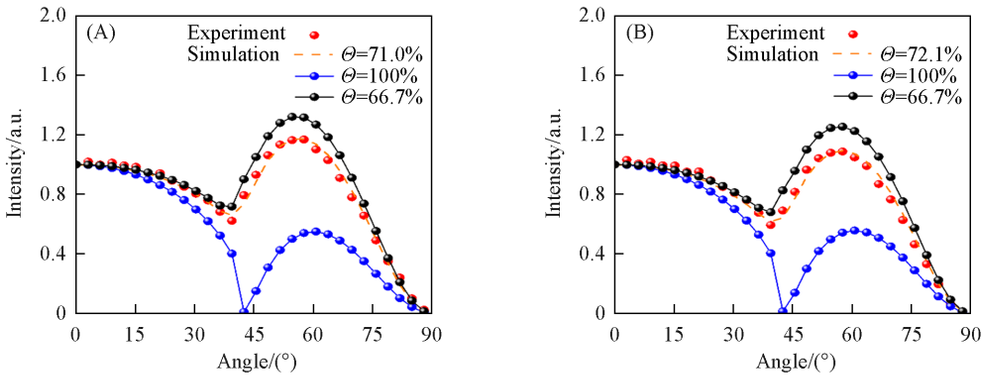


**Fig. 3 *p*-Polarized PL spectra of *m*CP-BP-PXZ(A) and *m*CBP-BP-PXZ(B) measured in neat films**

### 3.2 Bipolar Charge Transport Performance

To evaluate the carrier transport capabilities of *m*CP-BP-PXZ and *m*CBP-BP-PXZ in thick films, the mobilities of electron ($\mu_e$) and hole ($\mu_h$) are evaluated by the space-charge limited current (SCLC) method based on the electron- and hole-only device. Electron- and hole-only devices are fabricated with the configuration of ITO/TmPyPB(10 nm)/EML(80 nm)/TmPyPB(10 nm)/LiF(1 nm)/Al and ITO/TAPC(10 nm)/EML(80 nm)/TAPC(10 nm)/Al, respectively, where TAPC and TmPyPB function as buffer layers to shield off electrons and holes, respectively. The EMLs are the neat films of *m*CP-BP-PXZ or *m*CBP-BP-PXZ. As shown in Figs.4(A) and (B), the electron and hole current densities are similar, demonstrating balanced bipolar charge transport of *m*CP-BP-PXZ or *m*CBP-BP-PXZ. The $\mu_e$ and $\mu_h$ are fitted by the Mott-Gurney equation based on the current density-voltage curves [Figs.4(C) and (D)][42]. And the $\mu_e$ and $\mu_h$ are $6.74\times10^{-4}$ and $1.20\times10^{-3}$ $cm^2\cdot V^{-1}\cdot s^{-1}$ for *m*CP-BP-PXZ and $4.35\times10^{-4}$ and $9.34\times10^{-4}$ $cm^2\cdot V^{-1}\cdot s^{-1}$ for *m*CBP-BP-PXZ, respectively, at an electric field of $1.0\times10^6$ V/cm. Such balanced bipolar carrier transport capabilities of both emitters could suppress the shift of the recombination zone under high voltages and form a broad recombination zone[18,30,43]. When applied in thick-layer devices, the recombination zone will be broad enough to reduce the exciton concentration, thereby

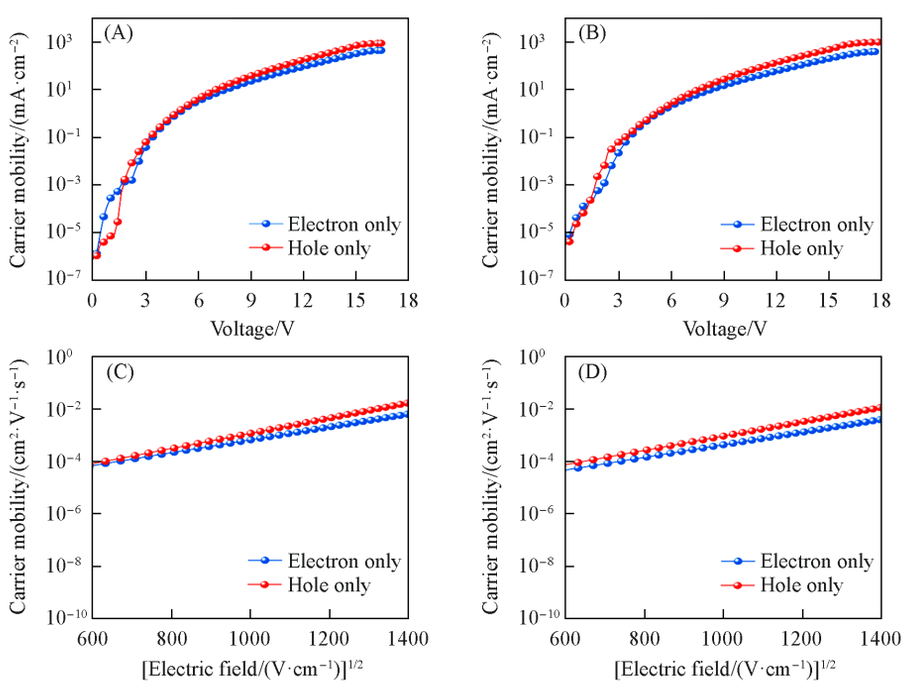


**Fig. 4 Plots of current density-voltage of single carrier devices of *m*CP-BP-PXZ(A) and *m*CBP-BP-PXZ(B) in neat films, and plots of electric field-dependent mobilities of *m*CP-BP-PXZ(C) and *m*CBP-BP-PXZ(D) in neat films**

improving device stability.

### 3.3 EL Performance

3.3.1 Complex Thin-layer Non-doped OLEDs To systematically study the effect of the thickness of emissive layer and the number of active layers on EL performance, the non-doped OLEDs based on *m*CP-BP-PXZ and *m*CBP-BP-PXZ with complex thin-layer and simple thick-layer configurations are fabricated initially. The configuration of the non-doped thin-layer devices is ITO/HATCN (5 nm)/TAPC (50 nm)/TcTa (5 nm)/EML(20 nm)/TmPyPB(40 nm)/LiF(1 nm)/Al. Here, dipyrazino[2,3-f:2′,3′-h]quinoxaline-2,3,6,7,10,11-hexacarbonitrile(HATCN), 4,4′-cyclohexylidenebis[*N*,*N*-bis(4-methylphenyl)aniline](TAPC), tris[4-(carbazol-9yl) phenyl]amine (TcTa) and 1,3,5-tri(m-pyrid-3-yl-phenyl)benzene (TmPyPB) work as hole-injection, hole-transporting, exciton-blocking and electron-transporting layers, respectively. The devices based on *m*CP-BP-PXZ and *m*CBP-BP-PXZ are referred to as Thin-I and Thin-II, respectively(Fig.5). All the devices are turned on at a low voltage of 2.5 eV and exhibit bright yellow-green light with the maximum luminance reaching up to 92290 and 82870 cd/m$^2$ for *m*CP-BP-PXZ and *m*CBP-BP-PXZ, respectively, indicative of the facile injection, transport and recombination of carriers. The EL spectra of these emitters are almost identical with the EL emission peaking at 540 nm for *m*CP-BP-PXZ and 538 nm for *m*CBP-BP-PXZ[Fig.5(B)]. The $EQE_{max}$ is 20.1% for the devices based on *m*CP-BP-PXZ and 22.0% for the devices based on *m*CBP-BP-PXZ with negligible efficiency roll-offs of only 2.0% and 3.2% at 1000 cd/m$^2$, respectively.

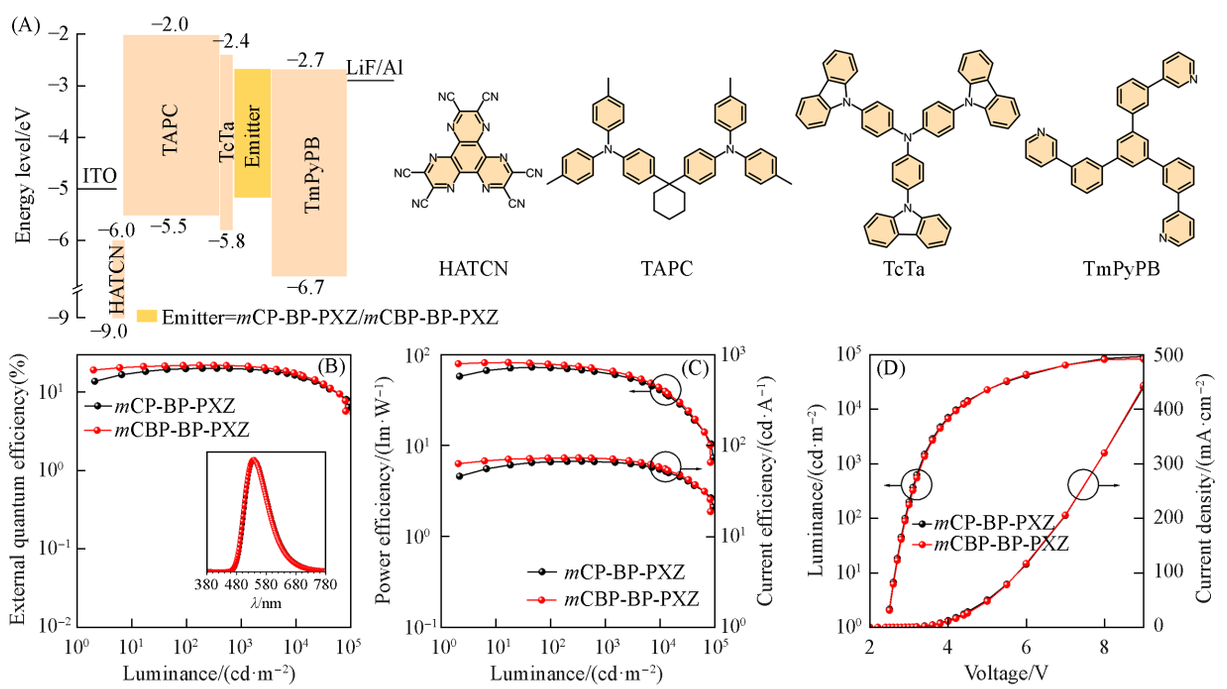


**Fig. 5 Configuration, energy diagram and molecular structures of the materials used in the thin-layer devices(A), plots of external quantum efficiency-luminance(B), power efficiency-luminance-current efficiency(C) and luminance-voltage-current density(D) of the non-doped thin-layer devices based on *m*CP-BP-PXZ and *m*CBP-BP-PXZ**

Inset in planes (B): EL spectra at 1000 cd/m$^2$ of thin-layer non-doped devices.

3.3.2 Simple Thick-layer Non-doped OLEDs Given the balanced bipolar carrier transport capabilities and the superior AIDF characteristics, the application potential of *m*CP-BP-PXZ and *m*CBP-BP-PXZ in thick-layer non-doped devices is investigated with a simple device configuration of ITO/$MoO_3$(6 nm)/EBL(10 nm)/EML(*x* nm)/HBL(10 nm)/LiF(1 nm)/Al, where EBL refers to the electron-blocking layer and HBL refers to the hole-blocking layer. The influences of the selection of EBL and HBL materials, as well as the thickness of

**Table 2 EL performances of non-doped OLEDs***

| Emitter | Device | $\lambda_{EL}$/nm | $V_{on}$/V | $L_{max}$/(cd·m$^{-2}$) | CIE($x$, $y$) | CE/(cd·A$^{-1}$) | PE/(lm·W$^{-1}$) | EQE(%) | RO(%) |
|---|---|---|---|---|---|---|---|---|---|
| | | | | | | Maximum value/at 1000 cd·m$^{-2}$/at 10000 cd·m$^{-2}$ | | | |
| *m*CP-BP-PXZ | Thin-I | 540 | 2.5 | 92290 | (0.37, 0.58) | 66.8/65.9/54.7 | 72.6/62.6/40.9 | 20.1/19.7/16.4 | 2.0 |
| | Thick-I-PPF(/*m*CBP) | 538 | 2.4 | 100800 | (0.38, 0.58) | 60.3/59.0/51.1 | 69.4/46.3/26.8 | 18.4/18.0/15.6 | 2.2 |
| | Thick-I-TSPO1 | 540 | 2.5 | 56580 | (0.38, 0.57) | 56.9/55.4/48.4 | 63.1/41.5/25.3 | 17.2/16.7/14.6 | 2.9 |
| | Thick-I-TPBi | 540 | 2.4 | 99030 | (0.38, 0.57) | 54.7/53.4/48.0 | 63.1/41.9/27.4 | 16.5/16.1/14.5 | 2.4 |
| | Thick-I-CBP | 538 | 2.4 | 96710 | (0.38, 0.58) | 55.8/54.4/47.2 | 64.4/45.0/27.0 | 17.0/16.6/14.4 | 2.4 |
| | Thick-I-*m*CP | 538 | 2.4 | 97750 | (0.37, 0.58) | 55.0/53.6/46.6 | 64.4/44.3/26.6 | 16.8/16.3/14.2 | 3.0 |
| | Thick-I-SimCP2 | 534 | 2.4 | 99370 | (0.37, 0.58) | 56.6/55.5/47.9 | 60.4/48.5/27.4 | 17.3/17.0/14.7 | 1.7 |
| *m*CBP-BP-PXZ | Thin-II | 538 | 2.5 | 82870 | (0.37, 0.58) | 73.3/71.1/58.5 | 82.1/65.7/43.7 | 22.0/21.3/17.5 | 3.2 |
| | Thick-II-PPF(/*m*CBP) | 532 | 2.5 | 74380 | (0.36, 0.58) | 62.7/61.0/51.5 | 71.6/47.9/27.0 | 19.1/18.6/15.7 | 2.6 |
| | Thick-II-TSPO1 | 534 | 2.5 | 21650 | (0.36, 0.58) | 60.1/58.1/47.4 | 69.7/40.6/21.3 | 18.3/17.7/14.5 | 3.3 |
| | Thick-II-TPBi | 532 | 2.5 | 92880 | (0.36, 0.58) | 53.4/52.3/44.7 | 59.5/43.2/25.5 | 16.3/16.0/13.7 | 1.8 |
| | Thick-II-CBP | 532 | 2.5 | 85710 | (0.36, 0.58) | 64.7/62.7/51.2 | 75.1/54.7/29.3 | 19.8/19.2/15.7 | 3.0 |
| | Thick-II-*m*CP | 532 | 2.5 | 76330 | (0.36, 0.58) | 60.3/59.2/48.0 | 65.3/49.0/25.2 | 18.5/18.1/14.7 | 2.2 |
| | Thick-II-SimCP2 | 532 | 2.5 | 83430 | (0.36, 0.58) | 57.0/54.7/44.9 | 65.5/40.9/21.7 | 17.4/16.7/13.8 | 4.0 |

* Abbreviations: $\lambda_{EL}$=EL peak at 1000 cd/m$^2$; $V_{on}$=turn-on voltage at 1 cd/m$^2$; $L_{max}$=maximum luminance; CIE=Commission Internationale del' Eclairage coordinates at 1000 cd/m$^2$; CE/PE/EQE=current efficiency/power efficiency/external quantum efficiency; RO=external quantum efficiency roll-off from the maximum values to that at 1000 cd/m$^2$.

EML, on EL performance are studied. All relevant exciton-blocking layer materials are present in Fig. S3(see the supporting information of this paper).

Firstly, the devices adopting 2,8-bis(diphenylphosphoryl)dibenzo[b,d]furan(PPF), diphenyl[4-(triphenylsilyl)phenyl]phosphine oxide(TSPO1), and 2,2′,2″-(1,3,5-benzenetriyl)tris(1-phenyl-1H- benzimidazole)(TPBi) as HBL materials and *m*CBP as the EBL material are fabricated with the configuration of ITO/$MoO_3$(6 nm)/*m*CBP(10 nm)/EML(60 nm)/HBL(10 nm)/LiF(1 nm)/Al(Fig. 6). The devices with *m*CP-BP-PXZ as emitters are named Thick-I-PPF, Thick-I-TSPO1, and Thick-I-TPBi, while those based on *m*CBP-BP-PXZ are named Thick-II-PPF, Thick-II-TSPO1, and Thick-II-TPBi. Thanks to the balanced bipolar carrier transport and the matched energy level between active layers, the turn-on voltages of these thick-layer devices are as low as 2.4—2.5 eV, similar to those in thin-layer devices. The EL performances of these thick-layer devices are comparable to their thin-layer counterparts, demonstrating the suitability of *m*CP-BP-PXZ and *m*CBP-BP-PXZ for such device architectures. The $\lambda_{EL}$s of the *m*CP-BP-PXZ-based thick-layer devices are similar to those in thin-layer devices, at around 540 nm. For *m*CBP-BP-PXZ, the $\lambda_{EL}$s of thick-layer devices are blue-shifted by *ca.* 6 nm relative to the thin-layer device, which might result from the shift of the exciton recombination zone. The best EL performance is afforded in the devices Thick-I-PPF and Thick-II-PPF, with the $EQE_{max}$, maximum current efficiency($CE_{max}$) and power efficiency($PE_{max}$) of 18.4%, 60.3 cd/A, 69.4 lm/W and 19.1%, 62.7 cd/A, 71.6 lm/W, respectively. Compared with the devices employing PPF and TSPO1, the devices adopt TPBi exhibit lower $EQE_{max}$s. This might be attributed to the higher HOMO energy level of TPBi, which results in insufficient hole-blocking ability. Although the $EQE_{max}$s of the TSPO1-based devices are satisfactory, the maximum luminance and efficiency roll-off of devices Thick-I-TSPO1 and Thick-II-TSPO1 are much inferior to others. Given that the LUMO energy level of TSPO1 is higher than the work function of the cathode, this behavior in TSPO1-based devices might be caused by the electron injection barrier, which will trigger the concentration quenching associated with polarons under high voltage. Ultimately, PPF is selected as the optimal HBL material.

Then, *m*CBP, *m*CP, 4,4′-bis(carbazol-9-yl)biphenyl(CBP), and 3,5-bis(9H-carbazol-9-yl)tetraphenylsilane(SimCP2) are selected to screen the optimal EBL materials. The thick-layer devices are fabricated

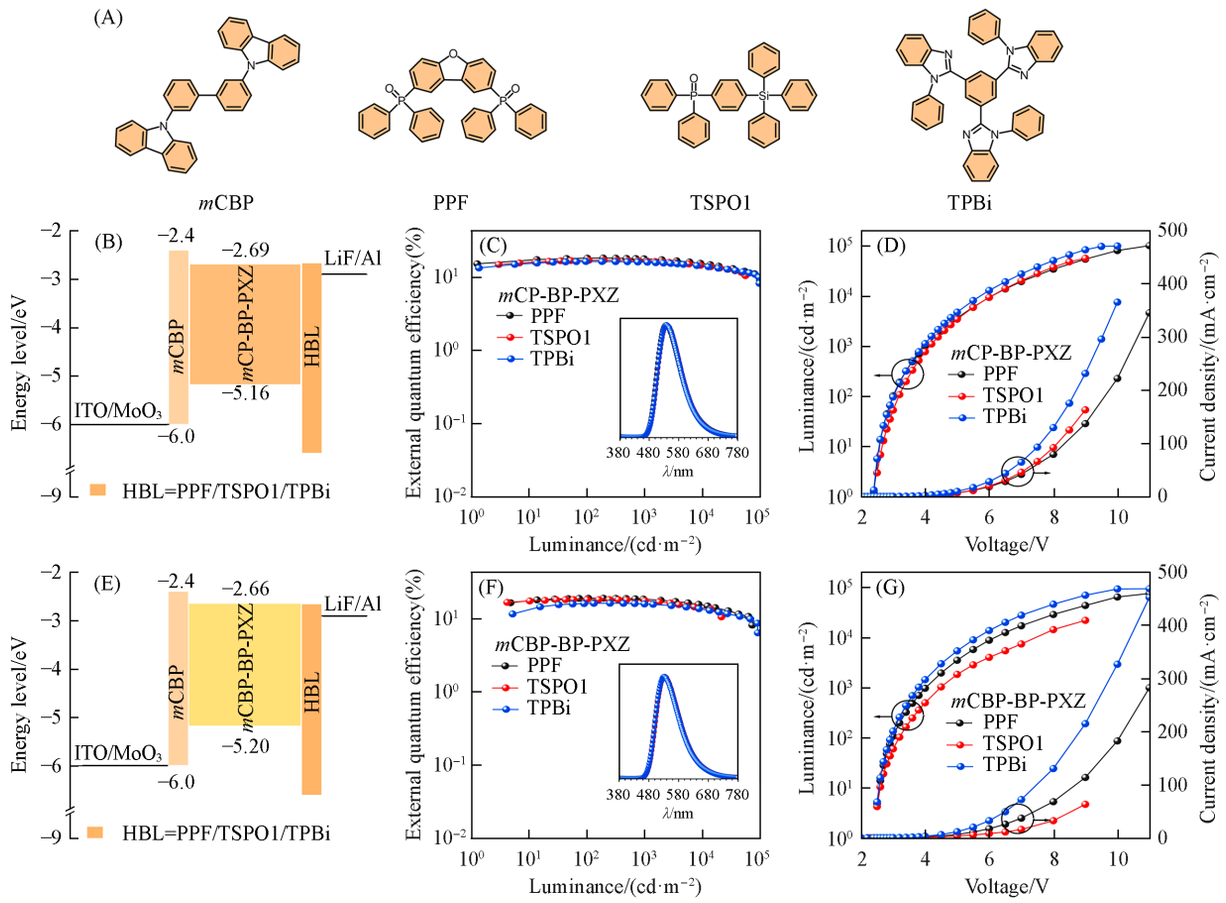


**Fig. 6 Molecular structures of the functional materials in the thick-layer non-doped devices with different HBL materials(A), configurations and energy level diagrams(B), plots of external quantum efficiency-luminance(C) and luminance-current density-voltage(D) of the *m*CP-BP-PXZ-based devices(Thick-I-HBL), configurations and energy level diagrams(E), plots of external quantum efficiency-luminance (F) and luminance-current density-voltage(G) of the *m*CBP-BP-PXZ-based devices(Thick-II-HBL)**

Insets in planes(C) and(F): EL spectra at 1000 cd/m$^2$ of thick-layer devices based on *m*CP-BP-PXZ and *m*CBP-BP-PXZ, respectively.

with the configuration of ITO/$MoO_3$(6 nm)/EBL(10 nm)/EML(60 nm)/PPF(10 nm)/LiF(1 nm)/Al(Fig.7). The devices employed *m*CP-BP-PXZ as emitters are referred to as Thick-I-*m*CBP, Thick-I-*m*CP, Thick-I-CBP, and Thick-I-SimCP2, while those based on *m*CBP-BP-PXZ are named Thick-II-*m*CBP, Thick-II-*m*CP, Thick-II-CBP, and Thick-II-SimCP2. The best EL performances of *m*CP-BP-PXZ and *m*CBP-BP-PXZ are afforded with *m*CBP and CBP functioning as EBL material, respectively. Thick-I-*m*CBP and Thick-II-CBP are turned-on at 2.4 and 2.5 V, with the maximum luminance reaching up to 100800 and 85710 cd/m$^2$, respectively. The $EQE_{max}$, $CE_{max}$ and $PE_{max}$ are 18.4%, 60.3 cd/A and 69.4 lm/W for the *m*CP-BP-PXZ-based device, and 19.8%, 64.7 cd/A and 75.1 lm/W for the *m*CBP-BP-PXZ-based device. The efficiency roll-offs of all devices at 1000 cd/m$^2$ are negligible, which are 2.2% for Thick-I-*m*CBP and 3.0% for Thick-II-CBP. The suppression of exciton annihilation at high voltage can be attributed to the fast RISC process and the brilliant AIDF properties.

The dependence of EL performance on the thicknesses of EML are further examined with the device configuration of ITO/$MoO_3$(6 nm)/*m*CBP(10 nm)/EML(*x* nm)/PPF(10 nm)/LiF(1 nm)/Al for *m*CP-BP-PXZ and of ITO/$MoO_3$(6 nm)/CBP(10 nm)/EML(*x* nm)/PPF(10 nm)/LiF(1 nm)/Al for *m*CBP-BP-PXZ(Fig.8). As the thickness of EML increases from 60 to 120 nm, all devices are turned-on at low voltages of around 2.5 V,

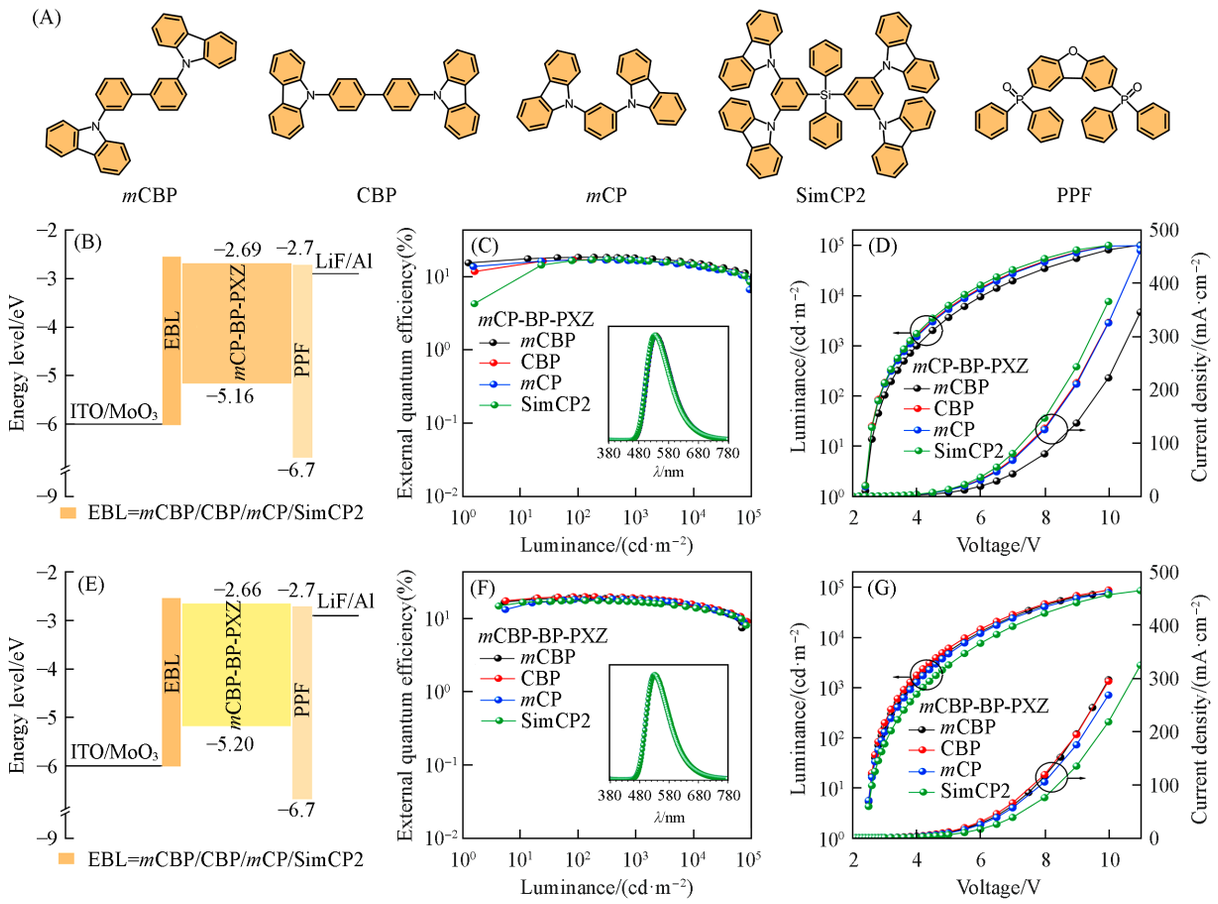


**Fig. 7 Molecular structures of the functional materials in the thick-layer non-doped devices with different EBL materials(A), configurations and energy level diagrams(B), plots of external quantum efficiency-luminance(C) and luminance-current density-voltage(D) of the *m*CP-BP-PXZ-based devices(Thick-I-EBL), configurations and energy level diagrams(E), plots of external quantum efficiency-luminance(F) and luminance-current density-voltage(G) of the *m*CBP-BP-PXZ-based devices(Thick-II-EBL)**

Insets in planes(C) and(F): EL spectra at 1000 cd/m$^2$ of thick-layer devices based on *m*CP-BP-PXZ and *m*CBP-BP-PXZ, respectively.

due to the balanced bipolar carrier transport. With the thickening of EML, the $\lambda_{EL}$s gradually red shift from 538 to 550 nm for *m*CP-BP-PXZ, and from 532 to 556 nm for *m*CBP-BP-PXZ, which can be attributed to the optical cavity effect resulting in a shift of the dominant wavelength for out-coupling. The optimal EML thickness is 80 nm for *m*CP-BP-PXZ and 60 nm for *m*CBP-BP-PXZ, and the corresponding $EQE_{max}$s are 18.4% and 19.8%, respectively. Notably, the $EQE_{max}$s remain as high as 16.3% even at 120 nm, exhibiting that the EQE can be maintained at a stable level across a wide range of EML thicknesses. Besides, the variations in EML thickness have no significant impact on efficiency roll-offs, which remain less than 5%.

Subsequently, the operational lifetime of the thick-layer non-doped devices for *m*CP-BP-PXZ and *m*CBP-BP-PXZ are evaluated based on the optimal HBL, EBL materials and EML thickness(Fig.9). The specific device configuration is ITO/$MoO_3$(6 nm)/*m*CBP(10 nm)/EML(80 nm)/PPF(10 nm)/LiF(1 nm)/Al for *m*CP-BP-PXZ and of ITO/$MoO_3$(6 nm)/CBP(10 nm)/EML(60 nm)/PPF(10 nm)/LiF(1 nm)/Al for *m*CBP-BP-PXZ. The thin-layer devices are also measured as a reference with the configuration of ITO/$MoO_3$(6 nm)/NPB(40 nm)/TcTa(5 nm)/EML(20 nm)/TPBi(40 nm)/LiF(1 nm)/Al(Fig.S1 and Table S1, see the Supporting Information of this paper). These thick-layer and thin-layer devices possess comparable $EQE_{max}$s of 18.4% and 20.1% for *m*CP-BP-PXZ, and 19.8% and 22.0% for *m*CBP-BP-PXZ, respectively, which keep at

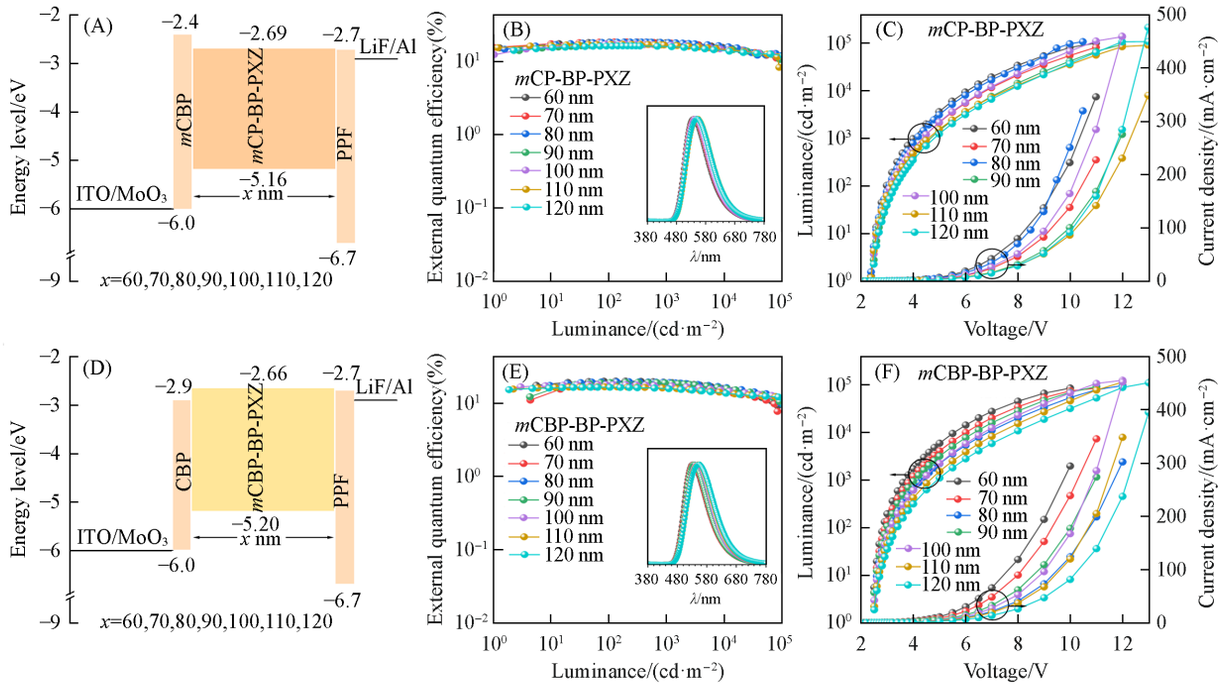


**Fig. 8 Configurations and energy level diagrams(A), plots of external quantum efficiency-luminance(B) and luminance-current density-voltage(C) of the *m*CP-BP-PXZ-based thick-layer devices, configurations and energy level diagrams(D), plots of external quantum efficiency-luminance(E) and luminance-current density-voltage(F) of the *m*CBP-BP-PXZ-based thick-layer devices**

Insets in planes(B) and(E): EL spectra at 1000 cd/m$^2$ of thick-layer devices with different thickness of EML based on *m*CP-BP-PXZ and *m*CBP-BP-PXZ, respectively.

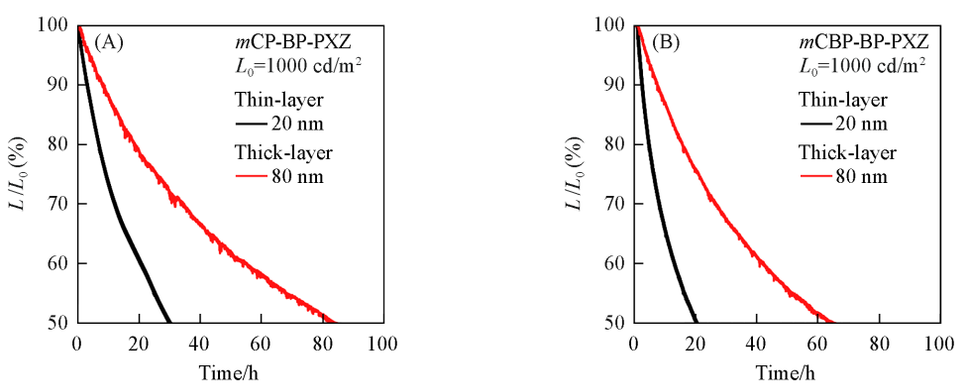


**Fig. 9 Operational lifetime of the non-doped thin-layer and thick-layer devices based on *m*CP-BP-PXZ(A) and *m*CBP-BP-PXZ(B)**

18.0% and 19.7% for *m*CP-BP-PXZ, and 19.2% and 21.3% for *m*CBP-BP-PXZ at 1000 cd/m$^2$. Under the initial luminance of 1000 cd/m$^2$, the operational lifetime to 50% initial luminance ($LT_{50}$) of both thick-layer devices are longer than those of thin-layer devices. For the thick-layer devices, the $LT_{50}$ is 83.5 h for *m*CP-BP-PXZ and 65.6 h for *m*CBP-BP-PXZ, representing one of the most stable thick-layer devices(Table S2, see the supporting information of this paper). While for the thin-layer devices, the $LT_{50}$s decrease by nearly half, which are only 30.2 h for *m*CP-BP-PXZ and 20.5 h for *m*CBP-BP-PXZ. The enhanced operational lifetime in thick-layer devices can be attributed to the decreased exciton density in a greatly broadened emission zone. Hence, thick-layer devices exhibit outstanding advantages in extending the operational lifetime. These impressive results reveal the great potential of the AIDF emitters for the application in the simple thick-layer device.

**Table 3 EL performances of the thick-layer non-doped OLEDs with different thickness of EML***

| Emitter | Thickness of EML/nm | $\lambda_{EL}$/nm | $V_{on}$/V | $L_{max}$/(cd·m$^{-2}$) | CIE($x$, $y$) | CE/(cd·A$^{-1}$) | PE/(lm·W$^{-1}$) | EQE(%) | RO(%) |
|---|---|---|---|---|---|---|---|---|---|
| | | | | | | Maximum value/at 1000 cd·m$^{-2}$/at 10000 cd·m$^{-2}$ | | | |
| *m*CP-BP-PXZ | 60 | 538 | 2.4 | 100800 | (0.38, 0.58) | 60.3/59.0/51.1 | 69.4/46.3/26.8 | 18.4/18.0/15.6 | 2.2 |
| | 70 | 540 | 2.4 | 81860 | (0.39, 0.57) | 60.6/58.6/49.9 | 69.4/40.9/22.4 | 18.4/17.8/15.2 | 3.3 |
| | 80 | 548 | 2.4 | 103200 | (0.40, 0.56) | 60.1/59.1/53.4 | 67.2/44.2/28.0 | 18.4/18.1/16.4 | 1.6 |
| | 90 | 550 | 2.5 | 93570 | (0.40, 0.56) | 55.2/54.7/49.1 | 59.3/38.2/22.1 | 17.0/16.9/15.2 | 0.6 |
| | 100 | 544 | 2.4 | 136900 | (0.39, 0.57) | 56.5/54.8/48.6 | 62.8/38.2/23.5 | 17.2/16.7/14.9 | 2.9 |
| | 110 | 550 | 2.4 | 91020 | (0.41, 0.55) | 54.8/53.6/47.7 | 64.6/37.4/21.4 | 17.2/16.8/15.0 | 2.3 |
| | 120 | 550 | 2.5 | 108600 | (0.41, 0.56) | 52.0/50.7/44.0 | 57.7/31.8/17.3 | 16.3/15.9/13.8 | 2.5 |
| *m*CBP-BP-PXZ | 60 | 532 | 2.5 | 85710 | (0.36, 0.58) | 64.7/62.7/51.2 | 75.1/54.7/29.3 | 19.8/19.2/15.7 | 3.0 |
| | 70 | 532 | 2.5 | 85060 | (0.36, 0.58) | 57.4/56.1/46.6 | 63.1/46.4/24.4 | 17.5/17.1/14.2 | 2.3 |
| | 80 | 534 | 2.6 | 96760 | (0.38, 0.57) | 64.0/62.7/53.1 | 70.3/46.9/23.8 | 19.4/19.1/16.1 | 1.5 |
| | 90 | 540 | 2.5 | 92290 | (0.37, 0.58) | 63.0/61.8/51.7 | 68.4/48.6/25.0 | 19.1/18.7/15.7 | 2.1 |
| | 100 | 550 | 2.5 | 124400 | (0.40, 0.56) | 57.7/55.1/48.5 | 67.1/38.5/23.4 | 17.8/17.0/15.0 | 4.5 |
| | 110 | 550 | 2.5 | 114400 | (0.41, 0.55) | 52.6/50.7/44.3 | 61.5/35.4/19.9 | 16.6/16.0/14.0 | 3.6 |
| | 120 | 556 | 2.5 | 111200 | (0.42, 0.55) | 51.3/48.9/42.1 | 59.6/30.7/16.5 | 16.3/15.6/13.5 | 4.3 |

* Abbreviations: $\lambda_{EL}$=EL peak at 1000 cd/m$^2$; $V_{on}$=turn-on voltage at 1 cd/m$^2$; $L_{max}$=maximum luminance; CIE=Commission Internationale de l'Eclairage coordinates at 1000 cd/m$^2$; CE/PE/EQE=current efficiency/power efficiency/external quantum efficiency; RO=external quantum efficiency roll-off from the maximum values to that at 1000 cd/m$^2$.

3.3.3 Simple Sensitized Thick-layer OLEDs To verify the sensitization capability of simplified thick-layer devices, BN3, a representative multi-resonance thermally activated delayed fluorescence (MR-TADF) molecule with an absorption peak at *ca.* 530 nm[44], is selected as the dopant, and employed in thick-layer sensitized device with the configurations of ITO/$MoO_3$(6 nm)/*m*CBP(10 nm)/1%(mass ratio) BN3∶*m*CP-BP-PXZ (60 nm) or 1%(mass ratio) BN3∶*m*CBP-BP-PXZ/PPF(10 nm)/LiF(1 nm)/Al(Fig. 10 and Table S3 in the supporting information of this paper). Both simple thick-layer sensitized OLEDs feature lower turn-on

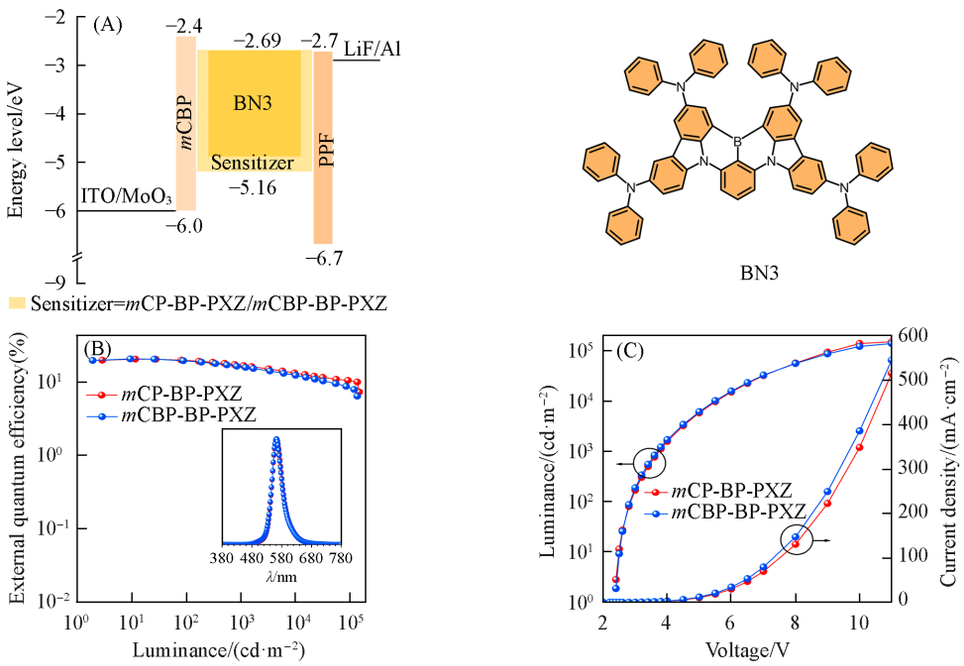


**Fig. 10 Configuration, energy diagram and molecular structure of the MR-TADF material used in the simple thick-layer sensitized devices(A), plots of external quantum efficiency-luminance(B) and luminance-voltage-current density(C) of the sensitized thick-layer devices**

Inset in planes(B): EL spectra at 1000 cd/m$^2$ of the thick-layer sensitized devices.

voltages of 2.4 V and high luminance exceeding 130000 cd/m$^2$. The EL peaks of sensitized devices center at *ca.* 562 nm with narrow FWHMs of *ca.* 40 nm and negligible shoulder peaks, demonstrating efficient Forster energy transfer from AIDF sensitizers to MR-TADF dopants. The corresponding CIE coordinates are (0.44, 0.55) for the *m*CP-BP-PXZ-based device and (0.43, 0.56) for the *m*CBP-BP-PXZ-based device. The $EQE_{max}$s of *m*CP-BP-PXZ and *m*CBP-BP-PXZ-based devices reach 20.8% and 20.9%, respectively, and remain at 17.0% and 16.6% at 1000 cd/m$^2$. These results clearly validate that the neat thick films of *m*CP-BP-PXZ and *m*CBP-BP-PXZ have the potential to sensitize MR-TADF emitters to afford high-efficiency, high-color-purity simplified thick-layer hyperfluorescence OLEDs.

## 4 Conclusions

In summary, two efficient AIDF emitters, *m*CP-BP-PXZ and *m*CBP-BP-PXZ, are successfully applied to fabricate high-performance simple thick-layer non-doped devices. Thanks to the balanced bipolar carrier transport, strong solid-state emission as well as fast RISC process, *m*CP-BP-PXZ and *m*CBP-BP-PXZ can serve the dual function of charge transport and light emission, meeting the essential requirements for application in the thick-layer devices. Despite the eliminated transport layers, the thick-layer non-doped devices maintain brilliant EL performance relative to the traditional multi-layer devices, which furnish bright yellow light with a low turn-on voltage of 2.4 V, high luminance of 100800 cd/m$^2$, and high $EQE_{max}$ of 18.4%, representing one of the state-of-the-art thick-layer OLEDs. Furthermore, the thick-layer devices based on *m*CP-BP-PXZ and *m*CBP-BP-PXZ exhibit excellent EL performance over a wide EML thickness range of 60 to 120 nm. Owing to the broadened exciton recombination zone and reduced exciton concentration, these thick-layer devices also enjoy outstanding operational stability with $LT_{50}$ lifetime of up to 83.5 h for *m*CP-BP-PXZ and 65.6 h for *m*CBP-BP-PXZ at 1000 cd/m$^2$ initial luminance, which are twice longer than those of thin-layer devices. Moreover, the neat thick films of *m*CP-BP-PXZ and *m*CBP-BP-PXZ can also function as sensitizers for MR-TADF emitter BN3 to prepare high-efficiency, high-color-purity simplified thick-layer hyperfluorescence OLEDs, providing good $EQE_{max}$s reaching 20.9% with small roll-offs. These results demonstrate that the thick-layer configuration is a feasible strategy for enhancing device stability, highlighting its great potential for applications in the OLED industry. Looking forward, thick-layer OLEDs based on bipolar AIDF materials hold significant promise for advancement through two pivotal strategies. Firstly, refining molecular design is imperative to achieve a higher horizontal dipole ratio, fast RISC processes, and balanced carrier transport, thereby enabling breakthroughs in both efficiency and stability. Secondly, extending the compatibility of the thick-layer architecture to organic light-emitting field-effect transistors and electrically pumped organic lasers, which would inject fresh momentum into the development of these fields.

The supporting information of this paper see http://www.cjcu.jlu.edu.cn/CN/10.7503/cjcu20260011.

## 参 考 文 献

[1] Tang C. W., VanSlyke S. A., *Appl. Phys. Lett.*, **1987**, *51*, 913—915
[2] Adachi C., Baldo M. A., Thompson M. E., Forrest S. R., *J. Appl. Phys.*, **2001**, *90*, 5048—5051
[3] Uoyama H., Goushi K., Shizu K., Nomura H., Adachi C., *Nature*, **2012**, *492*, 234—238
[4] Huang T., Wang Q., Zhang H., Zhang Y., Zhan G., Zhang D., Duan L., *Nat. Photon.*, **2024**, *18*, 516—523
[5] Jiang P., Miao J., Cao X., Xia H., Pan K., Hua T., Lv X., Huang Z., Zou Y., Yang C., *Adv. Mater.*, **2022**, *34*, 2106954
[6] Huang T., Xu Y., Qu Y., Lu X., Ye K., Zhuang X., Wang Y., *Adv. Mater.*, **2025**, *37*, 2503383
[7] Huang Z., Xie H., Miao J., Wei Y., Zou Y., Hua T., Cao X., Yang C., *J. Am. Chem. Soc.*, **2023**, *145*, 12550—12560
[8] Cheng Y. C., Tang X., Wang K., Xiong X., Fan X. C., Luo S., Walia R., Xie Y., Zhang T., Zhang D., Yu J., Chen X. K., Adachi C., Zhang X. H., *Nat. Commun.*, **2024**, *15*, 731
[9] Kido J., Kimura M., Nagai K., *Science*, **1995**, *267*, 1332—1334

[10] Walzer K., Maennig B., Pfeiffer M., Leo K., *Chem. Rev.*, **2007**, *107*, 1233—1271
[11] Kotadiya N. B., Wetzelaer G. J. A. H., Blom P. W. M., *Nat. Photon.*, **2019**, *13*, 765—769
[12] Sachnik O., Li Y., Tan X., Michels J. J., Blom P. W. M., Wetzelaer G. A. H., *Adv. Mater.*, **2023**, *35*, 2300574
[13] Hudson Z. M., Wang Z., Helander M. G., Lu Z., Wang S., *Adv. Mater.*, **2012**, *24*, 2922—2928
[14] Van der Zee B., Li Y., Wetzelaer G. J. A. H., Blom P. W. M., *Adv. Optical Mater.*, **2021**, *9*, 2100249
[15] Li Y., Kotadiya N. B., van der Zee B., Blom P. W. M., Wetzelaer G. A. H., *Adv. Optical Mater.*, **2021**, *9*, 2001812
[16] Li Y., Van der Zee B., Tan X., Zhou X., Wetzelaer G. J. A. H., Blom P. W. M., *Adv. Mater.*, **2023**, *35*, 2304728
[17] Fu Y., Liu H., Tang B. Z., Zhao Z., *Adv. Funct. Mater.*, **2024**, *34*, 2401434
[18] Liu Z., Guo T., Liu Z., Yang D., Ma D., Tang B. Z., Zhao Z., *Adv. Funct. Mater.*, **2026**, *36*, e17758
[19] Fu Y., Liu H., Zhu X., Zeng J., Zhao Z., Tang B. Z., *J. Mater. Chem. C*, **2020**, *8*, 9549—9557
[20] Wong M. Y., Zysman-Colman E., *Adv. Mater.*, **2017**, *29*, 1605444
[21] Hao X. L., Ren A. M., Zhou L., Zhang H., *J. Phys. Chem. A*, **2023**, *127*, 9771—9780
[22] Zhao M., Li M., Li W., Du S., Chen Z., Luo M., Qiu Y., Lu X., Yang S., Wang Z., Zhang J., Su S. J., Ge Z., *Angew. Chem. Int. Ed.*, **2022**, *61*, e202210687
[23] Guan J., Zhu Z., Gou Q., Wang J., Kuang Z., Zhang L., Zhang X., Ai X., Abdurahman A., Peng Q., *Aggregate*, **2025**, *6*, e70100
[24] Liu H., Guo J., Zhao Z., Tang B. Z., *ChemPhotoChem*, **2019**, *3*, 993—999
[25] Wang K., Ou X., Niu X., Wang Z., Song F., Dong X., Guo W., Peng H., Zhao Z., Lam J. W. Y., Sun J., Wu H., Yu S., Li F., Tang B. Z., *Aggregate*, **2025**, *6*, e667
[26] Ding Z., Wu B., Liu Z., Wang H., Gao F., Wei X., Zhao Z., Alam P., Qiu Z., Tang B. Z., *Aggregate*, **2025**, *6*, e70024
[27] Xu L., Li Y., Liu H., Qiu N., Chen H., Luo Y., Shi H., Zhao Z., Tang B. Z., *Aggregate*, **2026**, *7*, e70240
[28] Guo J., Zhao Z., Tang, B. Z., *Adv. Optical Mater.*, **2018**, *6*, 1800264.
[29] Huang J., Nie H., Zeng J., Zhuang Z., Gan S., Cai Y., Guo J., Su S., Zhao Z., Tang B. Z., *Angew. Chem. Int. Ed.*, **2017**, *56*, 12971—12976
[30] Xu J., Zhu X., Guo J., Fan J., Zeng J., Chen S., Zhao Z., Tang B. Z., *ACS Mater. Lett.*, **2019**, *1*, 613—619
[31] Guo J., Li X. L., Nie H., Luo W., Gan S., Hu S., Hu R., Qin A., Zhao Z., Su S. J., Tang B. Z., *Adv. Funct. Mater.*, **2017**, *27*, 1606458.
[32] Walia R., Xiong X., Fan X. C., Chen T. F., Wang H., Wang K., Shi Y. Z., Tang X., Bredas J. L., Adachi C., Chen X. K., Zhang X. H., *Nat. Mater.*, **2025**, *24*, 1576—1583
[33] Liu H., Zeng J., Guo J., Nie H., Zhao Z., Tang B. Z., *Angew. Chem. Int. Ed.*, **2018**, *57*, 9290—9294
[34] Liu Y., Li C., Ren Z., Yan S., Bryce M. R., *Nat. Rev. Mater.*, **2018**, *3*, 18020
[35] Goushi K., Yoshida K., Sato K., Adachi C., *Nat. Photon.*, **2012**, *6*, 253—258
[36] Zou Y., Yu M., Xu Y., Xiao Z., Song X., Hu Y., Xu Z., Zhong C., He J., Cao X., Li K., Miao J., Yang C. , *Chem*, **2024**, *10*, 1485—1501
[37] Zhang H., Huang T., Zhou J., Xu C., Zhang D., Duan L., *Chem*, **2025**, 102685
[38] Yokoyama D., *J. Mater. Chem.*, **2011**, *21*, 19187
[39] Zhao L., Komino T., Inoue M., Kim J. H., Ribierre J. C., Adachi C., *Appl. Phys. Lett.*, **2015**, *106*, 063301
[40] Fu Y., Liu H., Yang D., Ma D., Zhao Z., Tang B. Z., *Sci. Adv.*, **2021**, *7*, eabj2504
[41] Fan X., Wang K., Shi Y., Sun D., Chen J., Huang F., Wang H., Yu J., Lee C., Zhang X., *Smart Mat.*, **2023**, *4*, e1122
[42] Mott N. F., Gurney R. W., *Electronic Processes in Ionic Crystals*, the Clarendon Press, Oxford, **1940**
[43] Sachnik O., Ie Y., Ando N., Tan X., Blom P. W. M., Wetzelaer G. J. A. H., *Adv. Mater.*, **2024**, *36*, 2311892
[44] Qi Y., Ning W., Zou Y., Cao X., Gong S., Yang C., *Adv. Funct. Mater.*, **2021**, *31*, 2102017

(Ed.: F, K, V)